JAMES | Journal of Advances in Modeling Earth Systems

RESEARCH ARTICLE
10.1029/2020MS002431

Physics-Based Narrowband Optical Parameters for Snow Albedo Simulation in Climate Models

Wenli Wang[1], Cenlin He[2], John Moore[3,4], Gongxue Wang[5], and Guo-Yue Niu[6]

[1]Key Laboratory of Regional Climate-Environment Research for East Asia, Institute of Atmospheric Physics, Chinese Academy of Sciences, Beijing, China, [2]Research Applications Laboratory, National Center for Atmospheric Research, Boulder, CO, USA, [3]College of Global Change and Earth System Science, Beijing Normal University, Beijing, China, [4]Arctic Centre, University of Lapland, Rovaniemi, Finland, [5]Institute of Geospatial Information, Information Engineering University, Zhengzhou, China, [6]Department of Hydrology and Atmospheric Sciences, The University of Arizona, Tucson, AZ, USA

Key Points:

- The semi-empirical method used by Community Land Model to calculate narrowband snow optical parameters can produce errors that grow with snow mass
- The albedo errors stem from the relatively small biases in narrowband optical parameters that are amplified by nonlinear radiative transfer
- We propose a new set of narrowband snow optical parameters based on snow radiative transfer theory to improve albedo calculation accuracy

Correspondence to:
W. Wang,
wangwl@tea.ac.cn

Citation:
Wang, W., He, C., Moore, J., Wang, G., & Niu, G.-Y. (2022). Physics-based narrowband optical parameters for snow albedo simulation in climate models. *Journal of Advances in Modeling Earth Systems*, *14*, e2020MS002431. https://doi.org/10.1029/2020MS002431

Received 4 DEC 2020
Accepted 19 OCT 2021

Author Contributions:
Conceptualization: Wenli Wang
Formal analysis: Wenli Wang
Investigation: Wenli Wang
Methodology: Wenli Wang
Supervision: Guo-Yue Niu
Validation: Wenli Wang
Visualization: Gongxue Wang
Writing – original draft: Wenli Wang
Writing – review & editing: Cenlin He, John Moore, Guo-Yue Niu

Abstract Accurate snow albedo simulation is a prerequisite for climate models to produce reliable climate prediction. Climate models would benefit from schemes of snowpack radiative transfer that are responsive to changing atmospheric conditions. However, the uncertainties in the narrowband snow optical parameters used by these schemes have not been evaluated. Conventional methods typically compute these narrowband parameters as irradiance-weighted averages of the spectral snow optical parameters, with the single scattering albedo being additionally weighted by the optically thick snowpack albedo. We first evaluate the effectiveness of the conventional methods as adopted by the widely used Community Land Model (CLM). Snow albedo calculations using the CLM narrowband optical parameters are relatively accurate for very thin snow (e.g., a bias of 0.01 for a 2-cm snowpack). The error, however, becomes larger as snowpack thickens (with biases of up to 0.05 for semi-infinite snowpack), because the snow radiative transfer is highly nonlinear and is most significant at wavelengths <1 μm. In this study, we propose a novel method to retrieve broadband optical parameters according to snow radiative transfer theory, reducing the albedo biases to <0.003 for 2 cm snowpacks and <0.005 for thick snowpacks. We find little impact in changing incident spectra on narrowband snow albedo. These newly derived narrowband optical parameters improve snow albedo accuracy by a factor of 10, allowing to trace the impacts of aerosol pollution in snow. The parameters are independent of which two-stream approximation is used, and are thus applicable to sea ice, glaciers, and seasonal snow cover.

Plain Language Summary Snow albedo describes how much sunlight is reflected at the snow surface, which depends on how deep the sunlight penetrates the snowpack. Radiative transfer schemes describe sunlight absorption with snow optical depth. Snow radiative transfer schemes used in climate models make approximations using narrow-band snow optical properties for computational efficiency. A conventional way to derive the narrowband parameters is to average the wavelength-dependent values weighted by the incident solar spectrum. This approach produces snow albedo biases of up to 0.01 for shallow snowpacks and biases of up to 0.05 for thick snow. Such precision is not accurate enough for resolving the strongly positive snow-climate feedback when albedo decreases due to light-absorbing particles. This can amount to 0.01 over some "hot spots," which are climatically significant and have received increasing attention. Here, we provide a new set of narrowband optical parameters that improve the snow albedo accuracy by a factor of 10.

1. Introduction

Snow albedo describes how much incoming solar radiation is reflected at the snow surface. It is determined by microphysical processes in addition to the macroscopic structure of the snowpack. For example, the variation of snow grain radius and grain shape affect snow optics and the proportions of scattered and absorbed solar energy (Dang et al., 2015; He, Flanner, et al., 2018; Wiscombe & Warren, 1980). The light scattering capability of a snow grain particle is also dependent on the wavelength, λ, for example, ice is almost non-absorptive in the ultra violet and visible wavelengths, where the single scattering albedo (ω), that is, the ratio of scattering efficiency to extinction efficiency is close to 1, but drops nonlinearly at near infrared wavelengths.

As snow ages, the snow grain size increases and the albedo decreases. Under different temperature gradients, the snow grain would evolve into a ball or a lamellar structure (Rasmus, 2005). This metamorphic process results in stratified snow layers. Light-absorbing particles (LAPs) such as black carbon and mineral dust are enriched in the

upper snow layers as the snowpack melts. Since the LAPs absorb visible light better than pure snow, even at concentrations of a few parts per billion (Dang et al., 2017; Flanner et al., 2007, 2009; He, Liou, et al., 2018), changes in atmospheric loading and surface enrichment of LAPs are important for snow albedo variability over time.

Snow albedo is also dependent on illumination conditions and incident solar spectra. The radiative transfer treatment of direct light differs from that of diffuse light, as the direct solar beam acts as an external heating source to the snowpack that decays exponentially with snow optical depth (Toon et al., 1989). The solar zenith angle determines the path of direct sunlight and affects albedo (Aoki et al., 2003). The snow albedo under clear skies at all wavelengths increases with solar zenith angle (Wiscombe & Warren, 1980). The snow albedo under clear skies is lower than under cloudy skies for solar zenith angles <49.5° (Dang et al., 2015). Clouds, water vapor, and aerosols in the atmosphere reflect and absorb solar energy at various wavelengths, altering the incident solar spectrum reaching the snow surface. The mix of direct light and diffuse light therefore requires a merged solution in the snow radiative transfer scheme.

The positive snow-albedo feedback between reduced surface albedo and atmospheric warming (Déry & Brown, 2007; Fletcher et al., 2012; Hall & Qu, 2006) has accelerated Arctic sea ice melting and mountain glacier retreat (Hanesiak et al., 1999; Li et al., 2017; Ming et al., 2015). Physical properties of snow such as depth, density, grain size and shape, as well as the deposition of LAPs will change as a result of expected increases in future air temperatures and downward longwave radiation, reduced solid precipitation, and increased rain-on-snow events (Rasmus, 2005). Explicit treatment of snow micro-optical physics in the snow simulation modules used within climate models is needed to produce reliable macroscale characteristics, for example, snow cover fraction (Rasmus, 2005). To resolve the impacts of changing climate and LAPs on snow albedo requires snow albedo schemes of high, and as we shall show, higher accuracy than presently available in Land Surface Models (LSMs).

Snow radiative transfer requires calculation of: (a) snow-scattering properties, including single scattering albedo (ω), extinction coefficient (e), and asymmetry factor (g), which are independent of radiative transfer schemes (Bohren & Barkstrom, 1974) and (b) radiative transfer process (e.g., two-stream approximations), which solves for radiative fluxes through the snow layers for both direct and diffuse radiation.

Wiscombe and Warren (1980) developed a method to calculate spectrally resolved albedo across the 0.3–5 μm waveband for a homogeneous layer of pure snow. The nonspherical snow grains were represented by a collection of spheres with the same volume-to-area ratio (Giddings & LaChapelle, 1961). Flanner and Zender (2005) extended Wiscombe and Warren (1980) into a multilayer model (Snow, Ice, and Aerosol Radiative Model—SNICAR) by solving a tridiagonal matrix solution for the two-stream radiative transfer scheme (Toon et al., 1989). Eight species of LAP (Flanner et al., 2007) and four snow grain shapes (He, Flanner, et al., 2018) have also been incorporated within SNICAR.

Different from the radiative transfer approach, empirical or statistical formulations have been implemented into snow models to describe the evolution of snow albedo with time (Anderson, 1976). Some schemes include the effects of snow grain radius (Dang et al., 2015; Wang et al., 2020), grain shape (He et al., 2017; Liou et al., 2014), snow depth (Amaral et al., 2017; Wang et al., 2020) or snow density (Amaral et al., 2017), and LAPs (Dang et al., 2015; He, Liou, et al., 2018). These empirical schemes are unreliable for use in different environments and time periods because they are parameterized using limited observational data. Hence, empirical or semi-empirical approaches introduce various biases compared with the more process-based snowpack radiative transfer models (Wang, Yang, et al., 2021, companion manuscript).

A reduced complexity snow radiative transfer model is better suited for use in climate models to minimize computational cost. For example, instead of the 10 nm spectral resolution employed in SNICAR, the Community Land Model (CLM; Flanner et al., 2007) uses a version of SNICAR with five narrow wavebands (0.3–0.7, 0.7–1.0, 1–1.2, 1.2–1.5, and 1.5–5 μm). Over the five wavebands, CLM computes the optical parameters (discussed in detail in Section 2) of snow and LAP as irradiance-weighted averages of the spectral optical parameters (at 10 nm resolution), then additionally weighted-averaging the single scattering albedo with the albedo of optically thick snow (Flanner et al., 2007). The optical parameters over the five narrow wavebands used in CLM are rather effective for 2-cm-thick snow layers, producing an albedo bias within 0.01 relative to fine-resolution (10 nm) SNICAR. But the error rises with increasing snow mass, as this averaging method is semi-empirical (Flanner et al., 2007) and does not preserve the accuracy of the fine resolution (spectrally resolved) SNICAR in the resulting albedo over the five narrow wavebands. As more LSMs begin to adopt snow radiative transfer schemes for

snow albedo and snowpack internal heating calculations, improved understanding and uncertainty quantification of the narrowband snow optical parameters are desirable.

To address this problem, we propose a new physics-based method to reduce the biases in deriving narrowband snow optical parameters based on the snowpack radiative transfer theory. In Section 2, we analyze the Mie scattering properties of snow. We illustrate the albedo biases that are produced with the narrowband optical parameters currently used in CLM in Section 3. In Section 4, we introduce the physics-based methodology to derive a more accurate set of narrowband optical parameters for pure snow and LAPs. In Section 5, the accuracy of the newly derived narrowband snow optical parameters is examined, and uncertainties from both the spectrum of incident radiation and the nonlinearity of snow radiative transfer are discussed. The main message of this study is summarized in Section 6.

2. Spectral Characteristics of Mie Optical Properties of Snow

The Mie optical parameters represent the light scattering and absorption abilities of snow grains. When the incident sunlight reaches the snow particles, the mass extinction cross section (e, $m^2 \bullet kg^{-1}$) measures the hypothetical area normal to incident radiation per unit mass and gives total radiative flux scattered and absorbed by the snow particles. The mass scattering cross section (s, $m^2 \bullet kg^{-1}$) is the area that scatters the total radiant flux. The mass absorption cross section (b, $m^2 \bullet kg^{-1}$) is the area that absorbs and dissipates the total radiative flux. The single scattering albedo (ω) is the ratio of scattering cross section to extinction cross section. Asymmetry factor (g) is the mean of cosine of the scattering angle, integrated over the complete scattering phase function. An asymmetry factor of 1 means that light is scattered completely forward.

Most existing snow radiative transfer schemes use Mie optical properties as input (Bohren & Huffman, 1983; Meador & Weaver, 1980), including e, ω, and g. The three Mie optical properties are calculated from the snow complex refractive index, grain size, wavelength, and the number of scattering angles in a spherical space (Bohren & Huffman, 1983). The e and ω can be further transformed to or from other optical variables according to the following equations.

$$e_i = \frac{\tau_i}{z \cdot \rho} \tag{1}$$

$$\omega_i = \frac{s_i}{e_i} \tag{2}$$

$$b_i = e_i - s_i \tag{3}$$

$$co\text{-}\alpha_i = 1 - \omega_i \tag{4}$$

where the subscript i represents pure snow or species of LAP. τ is snow optical depth, z is snow depth in meter, and ρ is the snow density in $kg \cdot m^{-3}$. The sum of s and b is equal to e. e represents the light extinction capability of the snow layer. $co\text{-}\alpha$ is the single-scattering co-albedo. The scattering capability of the snowpack can be represented by either ω or s. The absorption capability of the snowpack can be described using either $co\text{-}\alpha$ or b.

As shown in Figure 1, solar energy peaks at visible wavelengths (Figures 1a and 1b). The spectral distribution of irradiance under a cloudy sky (Figure 1b) differs from that under a clear sky (Figure 1a) at wavelengths sensitive to vapor absorption, for example, 0.9 and 1.5 μm. Both the mass extinction cross section e (Figure 1c) and the asymmetry factor g (Figure 1d) vary much less, particularly at wavelengths <1.4 μm. In contrast, mass absorption cross section b varies by several orders of magnitude (Figure 1g), for wavelengths <1.4 μm, and b dominates the variability in the single scattering co-albedo $co\text{-}\alpha$ (Figure 1f). The single scattering albedo ω of ice grains is close to 0.5 where the strongest absorption occurs (Figure 1e).

3. Narrowband Snow Optical Parameters and Albedo Bias in CLM

3.1. Description of SNICAR Model and Solar Spectrum Data

The input parameters into SNICAR include incident radiation type (direct or diffuse), solar zenith angle, number of snow layers with thickness, density, and grain effective radius, grain shape in each layer, underlying ground

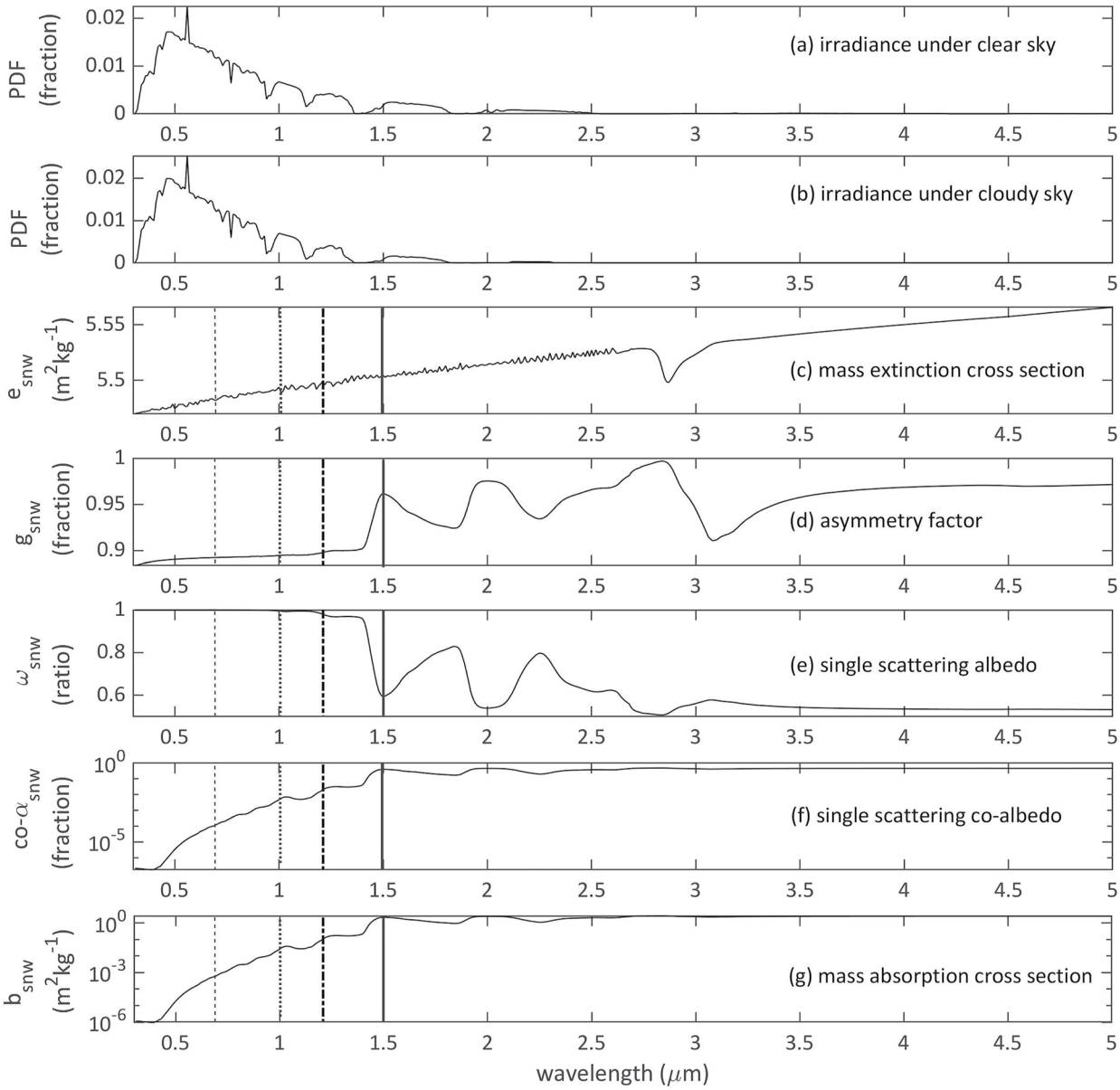

Figure 1. Probability density function (PDF), that is, spectral distribution of incoming solar irradiance under both (a) clear sky with solar zenith angle of 60° and (b) cloudy sky in a typical midlatitude winter, in fraction. (c–g) Wavelength-dependent Mie optical properties of 300 μm pure snow grain. (c–g)The five narrow bands divided in CLM are segmented by the vertical lines. The acquirement of surface spectrum data is described in detail in Section 3.1.

albedo, and aerosol concentrations in snow. The number of snow layers can be user-specified. As inputs to radiative transfer calculations, the Mie optical properties of snow grains and impurities have been computed and archived as lookup tables.

There are three choices for the two-stream approximation in SNICAR: Eddington, Quadrature, and Hemispheric mean. The three approximations differ in the assumption for scattering phase function, that is, distribution of scattering directions. There are four snow grain shapes in SNICAR: spherical, spheroidal, hexagonal plate, and Koch snowflake. The default SNICAR model assumes external mixing between impurities and snow grains. SNICAR does not consider focusing effects due to curved particle shapes, that is, the "ice lens" effect.

SNICAR uses clear- and cloudy-sky surface incident solar flux typical of midlatitude winter as the default solar spectra (Figures 1a and 1b). Surface spectral irradiances are calculated with the DISORT-based Shortwave

Narrowband (SWNB2) model (Zender, 1999; Zender et al., 1997), using standard atmospheric vertical profiles of water vapor, ozone, and other gases, and a lower-boundary spectral albedo typical of a snowpack with an effective grain size of 100 μm. The major differences in the atmospheric conditions between different spectra are vapor and cloudiness. The cloudy irradiances are modeled with a liquid cloud of optical thickness 10 at $\lambda = 500$ nm, located at a pressure of 800 hPa or in the bottom-most atmospheric layer of profiles with surface pressure less than 800 hPa. We evaluate the impact of variance in solar spectrum on narrowband snow albedo calculation in Section 5.2, including midlatitude winter, midlatitude summer, tropical, high mountain, subarctic winter, subarctic summer and summit Greenland. Spectrum data were obtained from the SNICAR database (https://github.com/mflanner/SNICARv3).

3.2. Application of SNICAR in This Study

The assumption of two-stream approximation, mixing state between impurities and snow grains, choice of snow grain shape, and employment of fixed surface spectrum data affect the calculated narrowband snow albedo by SNICAR, and hence the derivation of narrowband snow optical parameters in Section 4. Here, we give the derivation of narrowband snow optical parameters in terms of snow grain shape, separate the narrowband parameters under clear sky from that under cloudy sky. The narrowband parameters should be independent of the two-stream approximations, and we validate the derived narrowband parameters for the Eddington, Quadrature, and Hemispheric mean approximations in Section 5.1. We do not include the internal mixing state for LAP in pure snow grains in the derivations, and this might be considered as a new LAP in future work.

SNICAR calculates the spectral albedo, $\alpha(\lambda)$, at 470 wavelengths from 0.3 to 5 μm at an interval of 10 nm. The $\alpha(\lambda)$ are integrated with the incoming solar irradiance $I^{\downarrow}(\lambda)$ over the wavelength interval from λ_1 to λ_2 (Figures 1a and 1b) to calculate the narrowband snow albedo $\bar{\alpha}$:

$$\bar{\alpha} = \frac{\int_{\lambda_1}^{\lambda_2} \alpha(\lambda) I^{\downarrow}(\lambda) d\lambda}{\int_{\lambda_1}^{\lambda_2} I^{\downarrow}(\lambda) d\lambda} \tag{5}$$

$\bar{\alpha}$ approaches the true value of narrowband snow albedo as the spectral albedo $\alpha(\lambda)$ calculated with the two-stream framework is of high accuracy compared with observations.

We use SNICAR to calculate the estimated narrowband snow albedo, $\dot{\alpha}$, with the effective narrowband snow optical parameters used in CLM or the derived new set of parameters in this study as input. $\dot{\alpha}$ is validated against $\bar{\alpha}$ in the following sections.

3.3. Narrowband Optical Parameters and Albedo Bias

CLM uses the effective narrowband snow optical parameters, calculated as the weighted averages of spectral properties with Equations 6 and 7, as input to the SNICAR two-stream radiative transfer calculation. To acquire the narrowband parameters, CLM adopts the spectral distributions of solar irradiance under both clear sky with an solar zenith angle of 60° and cloudy sky that are typical of a midlatitude winter (Figures 1a and 1b) as weights in averaging the spectral Mie optical properties of snow across each of the five narrowband wavelengths, that is, 0.3–0.7, 0.7–1.0, 1–1.2, 1.2–1.5, and 1.5–5 μm (Flanner et al., 2007; Oleson et al., 2010).

In CLM, the effective narrowband mass-extinction cross section ($\bar{e}$) is weighted by the spectrum of the incoming solar irradiance $I^{\downarrow}(\lambda)$:

$$\bar{e} = \frac{\int_{\lambda_1}^{\lambda_2} e(\lambda) I^{\downarrow}(\lambda) d\lambda}{\int_{\lambda_1}^{\lambda_2} I^{\downarrow}(\lambda) d\lambda} \tag{6}$$

The effective narrowband single scattering albedo ($\bar{\omega}$) is further weighted by the albedo of an optically thick snowpack α_{sfc}^{∞} as:

Table 1
Bias of Clean Snow Albedo Under Clear Sky Estimated With the Effective Narrowband Parameters Used in CLM and Derived in This Study

	Bands	0.3–0.7 μm	0.7–1.0 μm	1.0–1.2 μm	1.2–1.4 μm[a]	1.4–5.0 μm[a]	Solar band[b]
Thin snow	CLM	≤0.001	≤0.01	≤0.005	≤0.03	≤0.035	≤0.01
	This study	≤0.0003	≤0.006	≤0.002	≤0.002	≤0.002	≤0.003
Thick snow	CLM	≤0.05	≤0.03	≤0.005	≤0.03	≤0.035	≤0.04
	This study	≤0.004	≤0.008	≤0.002	≤0.002	≤0.002	≤0.005

[a]The fourth narrowband in CLM is 1.2–1.5 μm, the fifth narrowband in CLM is 1.5–5.0 μm. [b]Solar band (0.4–5.0 μm) snow albedo is the average of the five narrowband snow albedos weighted by the spectrum of incident radiation (Figure 1a). The flux weights of the five narrow bands under clear sky is: 0.513, 0.24, 0.087, 0.05 (0.06 in CLM), and 0.11 (0.1 in CLM).

$$\bar{\omega} = \frac{\int_{\lambda_1}^{\lambda_2} \omega(\lambda) I^{\downarrow}(\lambda) \alpha_{sfc}^{\infty}(\lambda) d\lambda}{\int_{\lambda_1}^{\lambda_2} I^{\downarrow}(\lambda) \alpha_{sfc}^{\infty}(\lambda) d\lambda} \tag{7}$$

For a "thin snow" case (<2 cm in depth or snow mass <10 kg•m^{-2} at a density of 500 kg•m^{-3}), the estimated narrowband albedo biases by CLM (i.e., using the CLM narrowband snow optical parameters) under direct radiation (clear sky) are within 10^{-3} over the 0.3–0.7 μm and 10^{-2} over the 0.7–1.0 μm band. But the errors rise significantly with increasing snow mass, as detailed in Table 1. As a result, the broadband direct snow albedo biases across the entire solar spectrum (0.3–5 μm) in CLM are about 0.01 for thin snow and up to 0.04 for thick snow.

The estimated narrowband snow albedo biases under diffuse radiation (cloudy sky) presents similar patterns as those under direct radiation shown in Figure 2, but with relatively smaller errors (Table 2). The broadband diffuse albedo biases across the entire solar spectrum is 0.0035 for thin snow and 0.02 for a semi-infinite snowpack.

3.4. Explanation of the Narrowband Albedo Biases

The Mie optical properties of snow at a specific wavelength is independent of snow mass but the spectral snow albedo is dependent on both wavelength and snow mass as required by radiative transfer (Figure 3). The narrowband snow albedo of a specific snow mass estimated with Equation 5 is equivalent to the albedo at a certain wavelength within each narrow band, labeled as gray circles in Figure 3. If the radiative transfer process is approximately linear, then the equivalent-albedo wavelength (i.e., location of circles in *x*-axis), should be independent of snow mass. The larger the variation in equivalent-albedo wavelength with snow mass, the stronger the nonlinearity of radiative transfer. The variation of equivalent-albedo wavelength with snow mass is therefore an indicator of the nonlinearity of snow radiative transfer. There is a positive skewing of the equivalent-albedo wavelength with the increase of snow mass for the 0.3–0.7 μm band and a negative skewing of the equivalent-albedo wavelength with the increase of snow mass for the 0.7–1.0 μm band. As a result, using the snow optical properties at one equivalent-albedo wavelength to estimate the narrowband snow albedo for all different snow mass conditions will produce a nontrivial albedo bias for the first two bands.

Using the irradiance-weighted average to estimate the narrowband snow optical parameters is not physically defendable (Flanner et al., 2007) as the optical properties are nonlinearly correlated with snow albedo. This is most obvious in the 0.7–1.0 μm band, where the relatively small spectral variation in snow optical properties (Figure 1), produces a range of snow albedo from 0.3 to 0.8 across the band for snow masses >40 kg•m^{-2} (Figure 3b). But, the variation of spectral albedo is only 0.01 in the case of 1 kg•m^{-2} snow mass (Figure 3b). The change of optical parameters in the 0.7–1.0 μm band is much smaller than that in the 1.0–1.2 μm band (Figure 1), but the radiative transfer nonlinearity is much more significant in the 0.7–1.0 μm band. This suggests that the nonlinearity is also related to the snow scattering properties, that is, ω is higher in the 0.7–1.0 μm band. The spectral albedo at wavelengths >1.2 μm varies only slightly with snow mass, probably because the absorption is strongest (Figure 1).

Combining the irradiance-weighted average of spectral single scattering albedo with further weighting by the albedo of optically thick snow (α_{sfc}^{∞} in Equation 7), as is done in CLM (Equation 7; Flanner et al., 2007), can

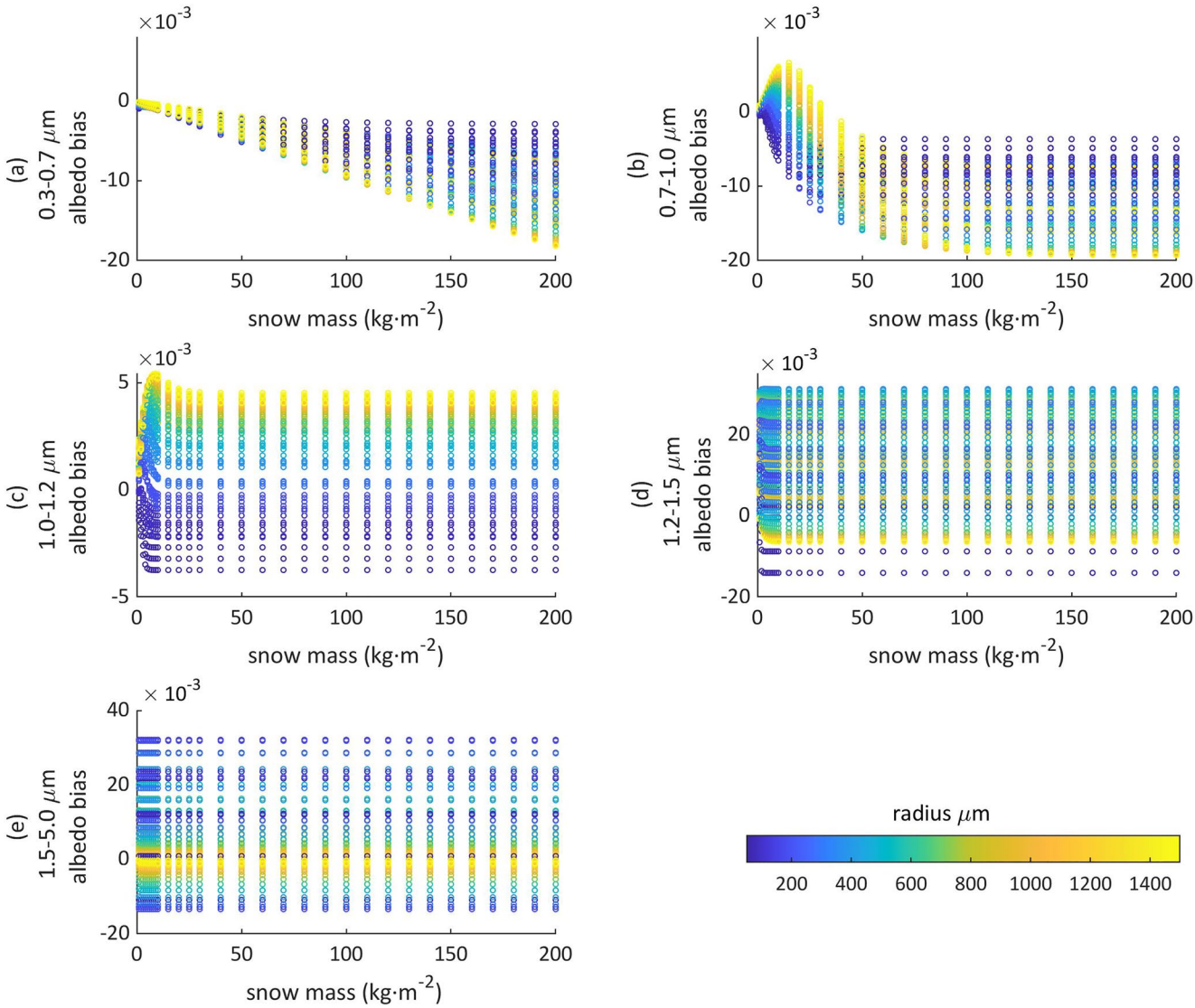

Figure 2. Biases in the narrowband clean snow albedo under direct incident radiation estimated with the five narrowband optical parameters in Community Land Model that are calculated with Equations 6 and 7, relative to the true value of narrowband snow albedos calculated with SNICAR as Equation 5. The snow grain radii ranges from 30 to 1,500 μm and are shown in colors. The albedo of bare ground below the snow layer is 0.2.

Table 2
Bias of Snow Albedo Under Cloudy Sky Estimated With the Effective Narrowband Parameters Used in CLM and Derived in This Study

	Bands	0.3–0.7 μm	0.7–1.0 μm	1.0–1.2 μm	1.2–1.4 μm[a]	1.4–5.0 μm[a]	Solar band[b]
Thin snow	CLM	≤0.001	≤0.006	≤0.005	≤0.015	≤0.005	≤0.004
	This study	≤0.0003	≤0.006	≤0.001	≤0.001	≤0.001	≤0.002
Thick snow	CLM	≤0.03	≤0.02	≤0.005	≤0.015	≤0.005	≤0.03
	This study	≤0.004	≤0.008	≤0.001	≤0.001	≤0.001	≤0.005

[a]The fourth narrowband in CLM is 1.2–1.5 μm, the fifth narrowband in CLM is 1.5–5.0 μm. [b]Solar band (0.4–5.0 μm) snow albedo is the average of the five narrowband snow albedos weighted by the spectrum of incident radiation (Figure 1b). The flux weights of the five narrow bands under cloudy sky is: 0.61, 0.25, 0.071, 0.033 (0.036 in CLM), and 0.036 (0.033 in CLM).

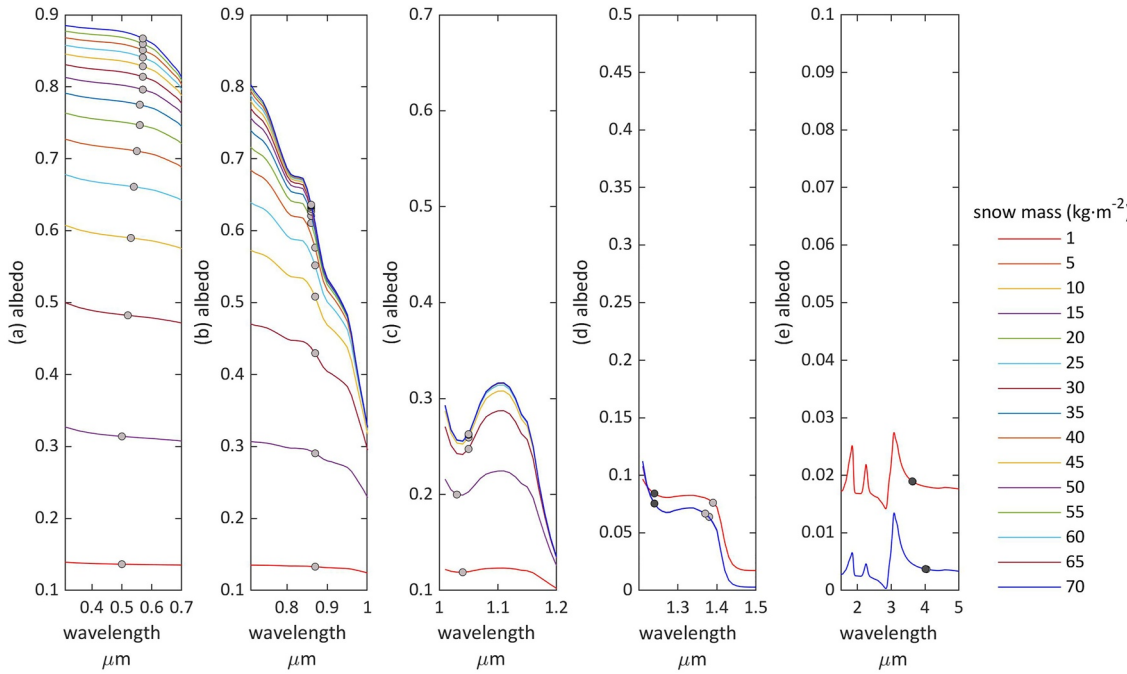

Figure 3. The wavelength-dependent clean snow albedo across each of the five narrow wavebands computed by SNICAR for different snow mass (legend) with grain radius of 1,300 μm. The corresponding narrowband albedos calculated with Equation 5 are labeled with gray circles. The snow albedos of the suggested reconfiguration of the fourth and fifth band boundary from 1.5 to 1.4 μm are shown as black circles for a 1.2–1.4 μm band in panel (d) and 1.4–5.0 μm band (the black circles overlap with the gray ones) in panel (e). The snow albedo curves for snow masses of 5–70 kg m^{-2} overlap each other in the fourth and fifth wavebands.

improve the accuracy of the estimated narrowband albedo (Figure 4b). The albedo of the optically thick snow, α^{∞}_{sfc}, is a function of the single scattering albedo (ω) and asymmetry factor (g), as discussed in Section 4. The application of α^{∞}_{sfc} to the calculation of narrowband ω will constrain the variation of ω with g and lower the estimated snow albedo bias. However, using the ω weighted with the albedo of optically thick snow instead of the direct relationship between ω and g is not accurate enough (see Section 3.3 and Figure 4). For example, the estimated albedo bias of thick snow for the 0.3–0.7 μm band (Figure 4a) using the irradiance-weighted ω further weighted with α^{∞}_{sfc} is less accurate than simply using the irradiance-weighted ω.

Adjusting the band boundary between the fourth and fifth CLM narrow bands from 1.5 to 1.4 μm produces a more accurate narrowband snow albedo estimate as the nonlinearity of the radiative transfer reduces, that is, the equivalent-albedo wavelengths in the 1.2–1.4 μm band are closer to each other compared with those of the 1.2–1.5 μm band (Figure 3d). We therefore recommend re-partitioning the fourth band as 1.2–1.4 μm and the fifth band as 1.4–5.0 μm. The re-partitioning of 1.4 μm was previously suggested by Fu (1996) to produce the narrowband parameters for ice clouds.

4. New Narrowband Snow Optical Parameters

4.1. Constraining ω With g

We want to find ω as a function of g because this helps us determine more realistic narrowband equivalent parameters. This can be done in several ways, but the simplest method is to use the analytical two-stream radiative transfer solution for the snow albedo under diffuse radiation (Wang, Moore, et al., 2021; second companion paper). The solution for the diffuse albedo is,

$$\alpha_{sfc} = k_1 + \Gamma \cdot k_2 \tag{8}$$

$$k_1 = \frac{\alpha_b \cdot \exp(-\lambda \cdot \tau_0) - \Gamma \cdot \exp(-\lambda \cdot \tau_0)}{\exp(\lambda \cdot \tau_0) - \Gamma^2 \cdot \exp(-\lambda \cdot \tau_0) - \alpha_b \cdot \Gamma \cdot \exp(\lambda \cdot \tau_0) + \alpha_b \cdot \Gamma \cdot \exp(-\lambda \cdot \tau_0)} \tag{9}$$

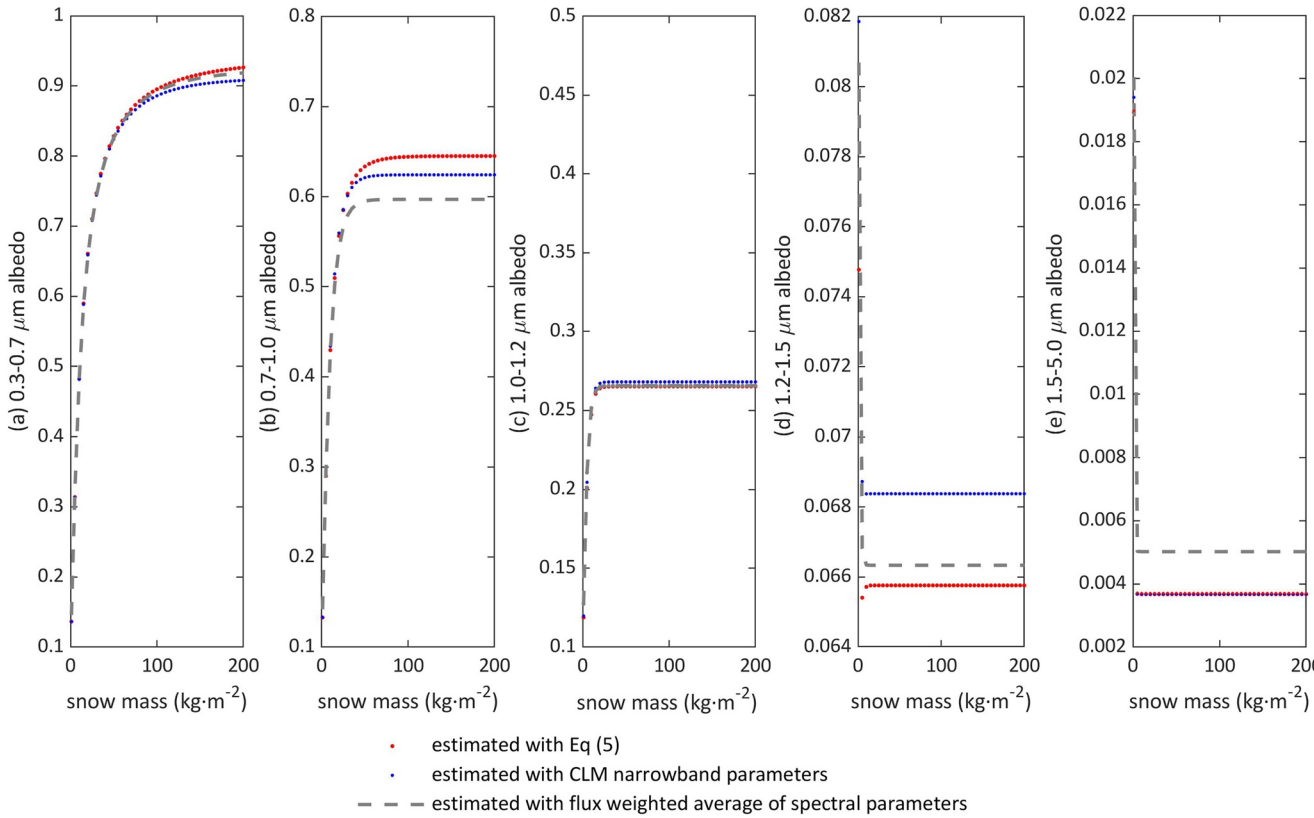

Figure 4. Narrow band clean snow albedos estimated with different parameters. The narrowband estimates from Equation 5 is regarded as truth (red dots). The estimated albedo from Community Land Model (blue dots) uses the flux-weighted spectral parameters (dashed gray lines) but with ω additionally weighted by α_{sfc}^{∞}, for the 1,300 μm snow grain demonstrated here.

$$k_2 = 1 - \Gamma \cdot k_1 \tag{10}$$

where α_{sfc} is the snow surface albedo, α_b is the bare ground albedo below snowpack, τ_0 is the optical depth of the snowpack, which can be calculated with Equation 1, λ and Γ are calculated as

$$\lambda = (\gamma_1^2 - \gamma_2^2)^{1/2} \tag{11}$$

$$\Gamma = \frac{\gamma_2}{(\gamma_1 + \lambda)} = \frac{\gamma_1 - \lambda}{\gamma_2} \tag{12}$$

γ_1 and γ_2 depend on the form of the two-stream approximation used.

For semi-infinite snow, $\tau_0 \to \infty$, $k_1 = 0$, $k_2 = 1$, and

$$\alpha_{sfc}^{\infty} = \Gamma \tag{13}$$

For the hemispheric mean approximation,

$$\gamma_1 = 2 - \omega(1 + g) \tag{14}$$

$$\gamma_2 = \omega(1 - g) \tag{15}$$

Solving Equations 11–15, ω can be organized in the form of α_{sfc}^{∞} and g as,

$$\omega = \frac{4 \cdot \alpha_{sfc}^{\infty}}{(1 - g) + 2 \cdot \alpha_{sfc}^{\infty} \cdot (1 + g) + \alpha_{sfc}^{\infty\,2} \cdot (1 - g)} \tag{16}$$

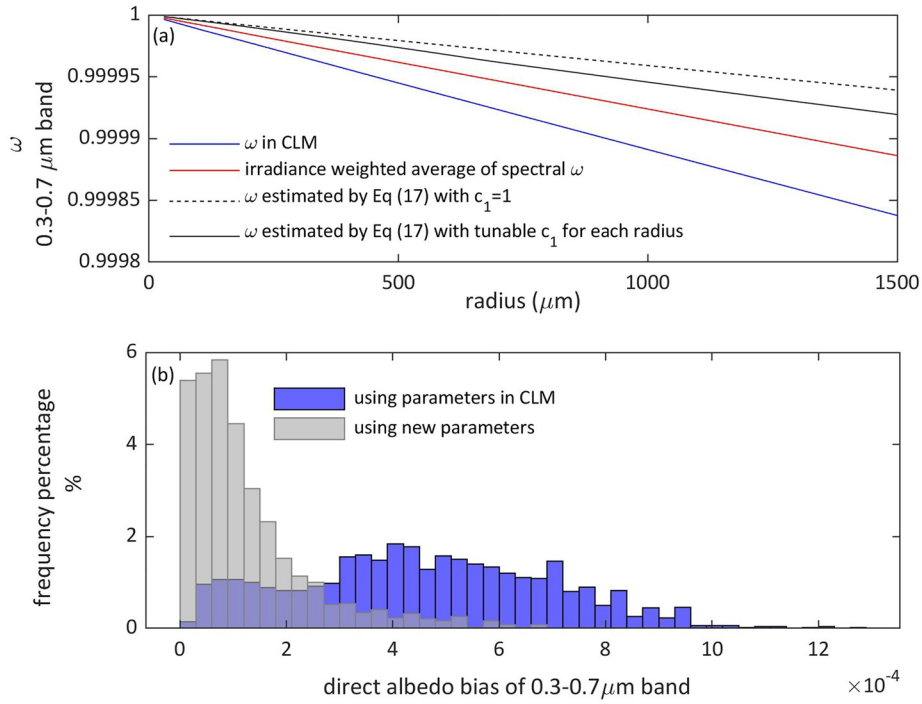

Figure 5. (a) 0.3–0.7 μm band single scattering albedo ω and (b) the bias distribution of estimated clean snow albedo for 2,000 snowpacks uniformly distributed in the range 0–10 kg•m^{-2} resulting from using narrowband parameters in CLM and using the tunable parameter c_1 with Equation 17 to minimize the narrow band albedo bias. The irradiance-weighted average of wavelength dependent albedo calculated with SNICAR as Equation 5 is regarded as the "truth".

Using other two-stream approximations and the analytical solution to direct radiation will deduce a much more complex form of Equation 16 for ω, g, and α_{sfc}^{∞}. We therefore use Equation 16 to constrain the narrowband parameters.

4.2. Derivation of Narrowband Optical Parameters of Pure Snow

As indicated by Figure 3, the best-fit wavelength-dependent snow optical parameters for the narrowband albedo of thick snow should differ from those of thin snow, and the difference should be especially significant for the 0.3–0.7 μm band and 0.7–1.0 μm band. The relationship between ω and g derived from a semi-infinite snowpack (Section 4.1) cannot be directly applied to thin snow. We propose to adjust the relationship of semi-infinite snow albedo with a coefficient, c_1,

$$\omega = \frac{4 \cdot \alpha_{sfc}^{\infty}}{(1 - c_1 \cdot g) + 2 \cdot \alpha_{sfc}^{\infty} \cdot (1 + c_1 \cdot g) + {\alpha_{sfc}^{\infty}}^2 \cdot (1 - c_1 \cdot g)} \tag{17}$$

c_1 can be optimized during parameter retrieval. Figure 5a shows the difference in ω calculated with different methods as a function of grain radius. Figure 5b shows that using a grain radius tunable c_1 coefficient (varying between 0.96 and 1.02) reduces bias in snow albedo by an order of magnitude compared with CLM.

The narrowband extinction coefficient and asymmetry factor can be estimated with the irradiance-weighted average of their spectrally resolved values. To further improve the accuracy, adjustments of the weighted average are applied as

$$\bar{e} = \frac{\int_{\lambda_1}^{\lambda_2} e(\lambda) \boldsymbol{I}^{\downarrow}(\lambda) d\lambda}{\int_{\lambda_1}^{\lambda_2} \boldsymbol{I}^{\downarrow}(\lambda) d\lambda} \cdot c_2 \tag{18}$$

$$\bar{g} = \frac{\int_{\lambda_1}^{\lambda_2} g(\lambda) I^{\downarrow}(\lambda) d\lambda}{\int_{\lambda_1}^{\lambda_2} I^{\downarrow}(\lambda) d\lambda} \cdot c_3 \tag{19}$$

c_2 and c_3 are also tunable and optimized during parameter retrieval. We find that $0.98 < c_i < 1.01$ for $i = 2$ and 3 in the 0.3–0.7, 0.7–1.0, 1.0–1.2, and 1.2–1.4 μm bands, and c_i is between 0.2 and 2 for the 1.4–5.0 μm band.

The specific values of c_1, c_2, and c_3 and hence the snow optical parameters (Equations 17–19) are optimized simultaneously in a 10^9 member Monte Carlo ensemble for each snow grain radius varying from 50 to 1,500 μm at an interval of 1 μm for various snow states (snow mass and solar zenith angles), and Eddington, Quadrature, and Hemispheric mean approximations.

We derive parameters for spherical, spheroidal, hexagonal plate, and Koch snow grain shapes as recently introduced in SNICAR (He, Flanner, et al., 2018). The different snow grain shapes with the same effective grain size predominantly affect the asymmetry factor g, with negligible effects on the extinction and absorption parameters (He & Flanner, 2020; Jin et al., 2008; Räisänen et al., 2015). The estimated extinction coefficient and single scattering albedo of spherical snow grain can hence be used for the other three snow grain shapes. Therefore, we optimize just c_3 in Equation 19 with Monte Carlo methods to get the effective narrowband asymmetry factors of the spheroidal, hexagonal plate, and Koch snowflake. The newly derived narrowband optical parameters significantly improve the accuracy of narrowband albedo for both thin and thick snow cases by a factor of two, and by an order of magnitude, respectively, for all narrow bands, and will be examined in more detail in Section 5.

4.3. Derivation of Narrowband Optical Properties of LAPs

The absorption of sunlight by natural snow at the visible wavelengths is mainly due to LAPs that are incorporated in snowpack through both wet processes in snowfall and by dry deposition directly onto the snow surface (Dang et al., 2015). Figure 6 shows the Mie optical properties of two black carbon (BC) species (i.e., pure BC and sulfate-coated BC), mineral dust at four size bins (i.e., 0.05–0.5, 0.5–1.25, 1.25–2.5, and of 2.5–5.0 μm radius), and one species of volcanic ash, as defined in SNICAR and CLM and as also applied in global aerosol transport studies (Mahowald et al., 2006; Scanza et al., 2015; Zender et al., 2003).

In many parts of the world, black carbon (BC) is the most important LAP, but the concentration of BC in a snowpack can vary by several orders of magnitude, from ∼10 ng/g in the Antarctic and Arctic to ∼100 ng/g in the interior of Tibetan Plateau and ∼1,000 ng/g in the northeast of China (Clarke & Noone, 1985; Dang et al., 2017; He, Flanner, et al., 2018; Huang et al., 2011; Warren & Clarke, 1990). In other places like Mongolia and the western USA, mineral dust is the dominant LAP in snow (Doherty et al., 2013, 2014; Painter et al., 2007; Wang et al., 2013; Zhang et al., 2013).

The absorption capability of mineral dusts is far less than BC but the concentration of dust can be higher than BC by several orders of magnitude in natural snow, 0.1–100 μg/g (Zhong et al., 2019). Explosive volcanism may deposit ash over great distances due to stratospheric transport (e.g., Gelman Constantin et al., 2020). The light absorption capability of volcanic ash is comparable to that of mineral dust but differs in its spectral distribution (Figure 6).

The retrieval of the effective narrowband optical properties of LAPs follows the same methodology as for pure snow (Section 4.2). Specifically, the narrowband optical properties of dirty snow (i.e., snow mixed with LAPs) is optimized by minimizing the biases of the resulting narrowband dirty snow albedo relative to the "true" narrowband albedo derived from the spectrally resolved radiative transfer calculation as Equation 5. Then, the narrowband pure snow parameter values optimized in Section 4.2 are subtracted from the derived narrowband optical parameter values of dirty snow (i.e., snow mixed with LAPs) with necessary weights to obtain the narrowband LAP optical parameters based on the following equations (Flanner et al., 2007):

$$\tau_{\text{snw+LAP}} = \tau_{\text{snw}} + \tau_{\text{LAP}} \tag{20}$$

$$\omega_{\text{snw+LAP}} = \frac{\tau_{\text{snw}}\omega_{\text{snw}} + \tau_{\text{LAP}}\omega_{\text{LAP}}}{\tau_{\text{snw}} + \tau_{\text{LAP}}} \tag{21}$$

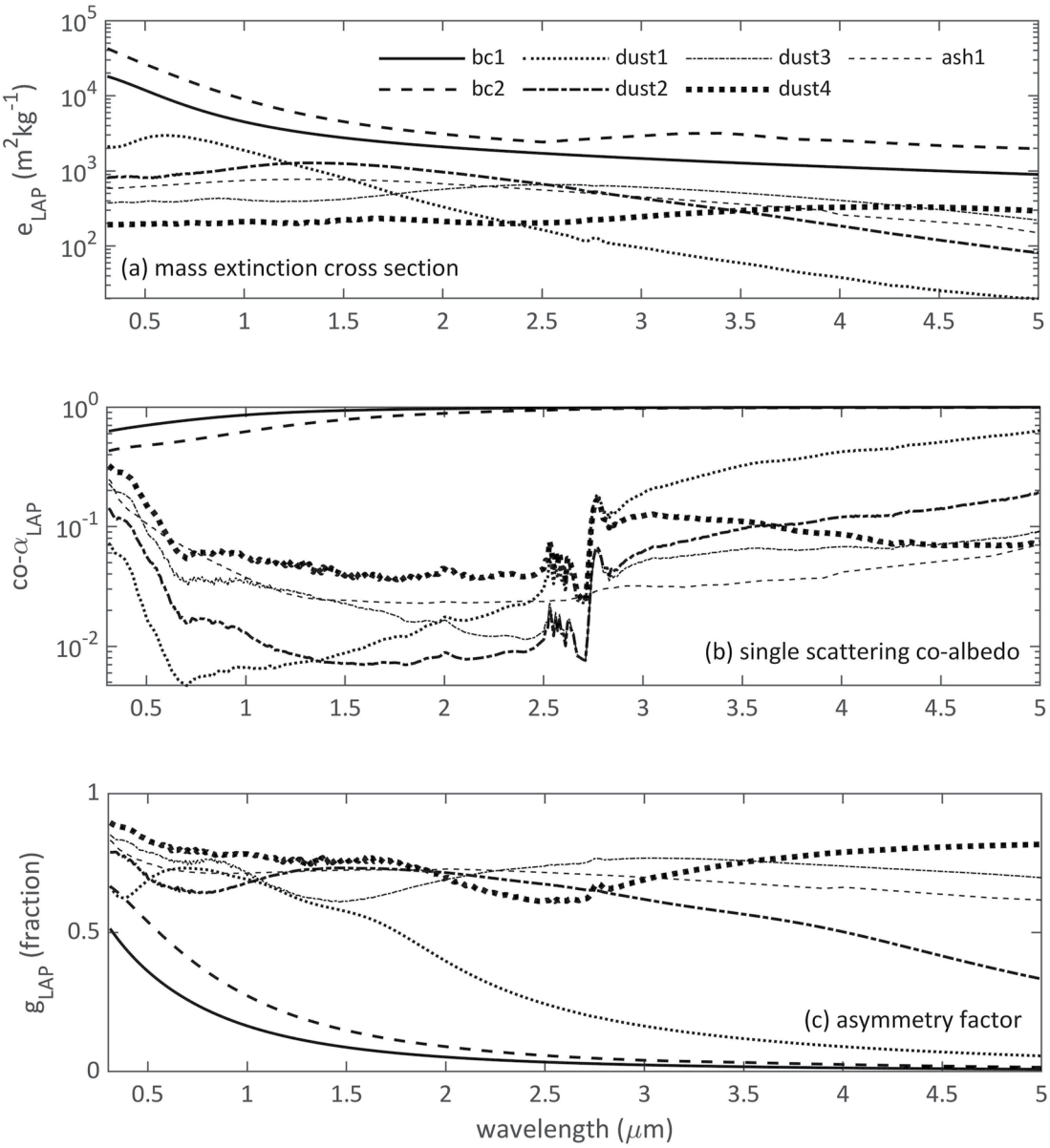

Figure 6. (a) The mass extinction cross section, (b) single scattering co-albedo, and (c) asymmetry factor of seven species of light-absorbing particles (LAPs). BC1 represents pure BC, BC2 represents self-coated BC. Dust1-4 represents dust species at four size bins. Specifically, dust 1 is of 0.05–0.5 μm radius, dust 2 is of 0.5–1.25 μm radius, dust 3 is of 1.25–2.5 μm radius, and dust 4 is of 2.5–5.0 μm radius. Ash1 represents volcanic ash.

$$g_{\mathrm{snw+LAP}} = \frac{\tau_{\mathrm{snw}}\omega_{\mathrm{snw}}g_{\mathrm{snw}} + \tau_{\mathrm{LAP}}\omega_{\mathrm{LAP}}g_{\mathrm{LAP}}}{\tau_{\mathrm{snw}}\omega_{\mathrm{snw}} + \tau_{\mathrm{LAP}}\omega_{\mathrm{LAP}}} \tag{22}$$

The resulting narrowband LAP optical properties are similar to the commonly used irradiance-weighted average of the spectral values. Our derived new narrowband optical properties of both pure snow and LAPs are stored in a lookup table, which can then be used by climate models for snow albedo calculations. The derived parameters are available at https://doi.org/10.5281/zenodo.4305014.

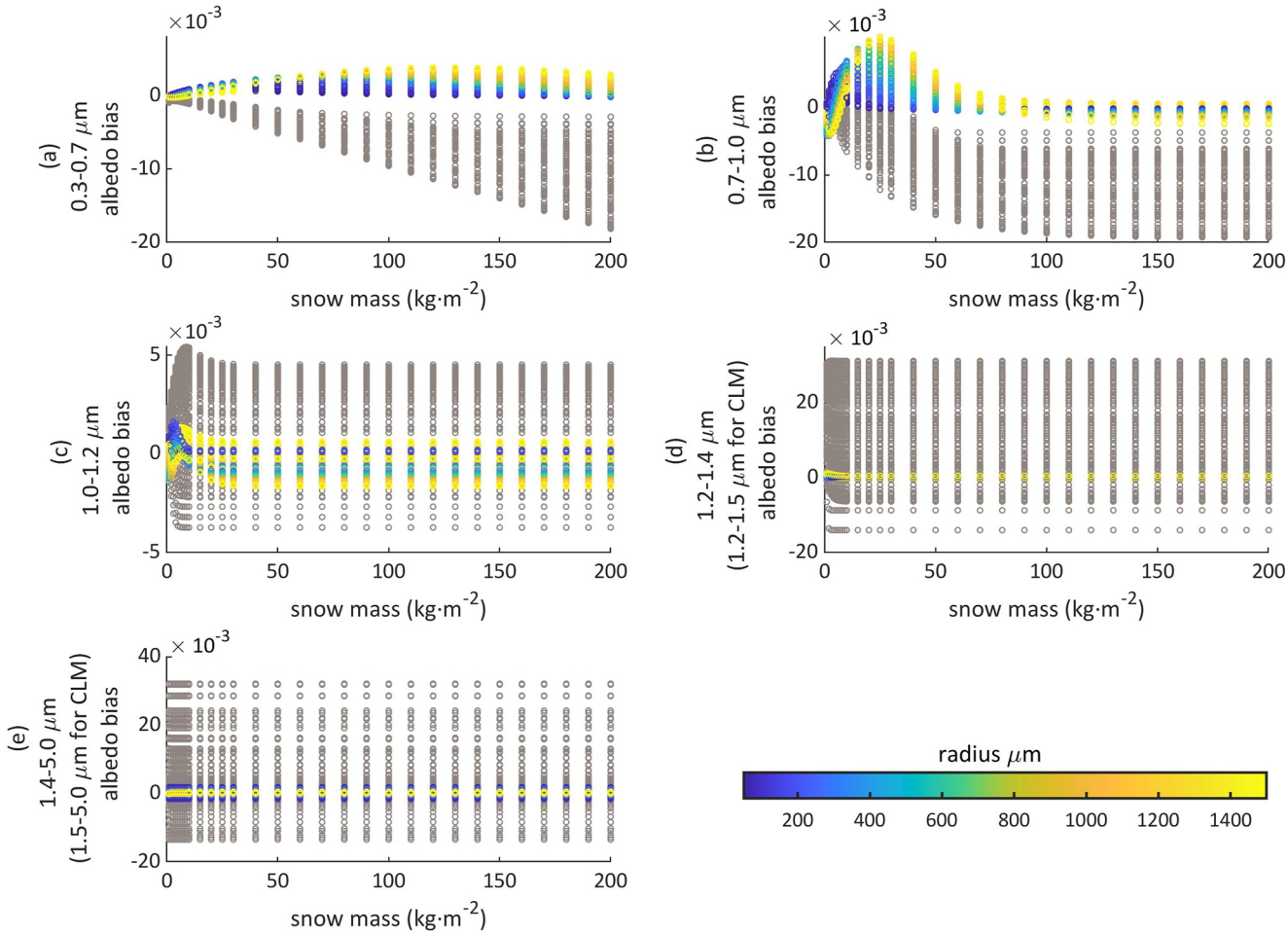

Figure 7. The error in the narrowband clear-sky clean snow albedo for the Eddington, Quadrature, and Hemispheric mean approximations estimated with the newly derived effective parameters with Equations 17–19, shown in colors indicating snow grain radius. The Community Land Model errors are shown in gray. The spectrally resolved snow albedos calculated by SNICAR are integrated with the incident solar flux to estimate the "true" narrowband snow albedo as Equation 5. The albedo of bare ground below the snow layer is 0.2.

5. Evaluation and Uncertainty Quantification

5.1. Improved Accuracy Using New Optical Parameters

Small biases in the estimated narrowband snow optical parameters can lead to large errors in the narrowband albedo due to the nonlinearity of radiative transfer (Figure 3). We introduce the relationship between single scattering albedo ω and asymmetry factor g from the diffuse albedo of semi-infinite snow to reduce the biases in deriving the narrowband snow optical parameters with Equations 17–19. The accuracy of the estimated narrowband albedo is greatly improved under both clear sky (Figure 7; Table 1) and cloudy sky conditions (Figure 8; Table 2) particularly for a thick snowpack.

Assuming the incoming solar radiation is 300 Wm^{-2}, the largest clear-sky albedo bias for the solar broadband using the new optical parameters is 0.005, equivalent to 1.5 Wm^{-2}, an improvement in albedo accuracy by a factor of eight compared with the bias of 0.04 using the parameters in CLM (Table 1), equivalent to 12 Wm^{-2} The largest cloudy-sky albedo bias for the solar broadband using the new optical parameters is 0.005, equivalent to 1.5 Wm^{-2}, compared with the bias of 0.02 using the parameters in CLM, equivalent to 6 Wm^{-2}.

For the thin snowpack at the top snow layer, the clear-sky clean snow albedo bias for the solar broadband using the new parameters is 0.003, equivalent to 0.9 Wm^{-2} in terms of incoming solar energy, compared with the albedo bias of 0.01 in CLM, equivalent to 3 Wm^{-2}; the cloudy-sky clean snow albedo bias for the solar broadband using

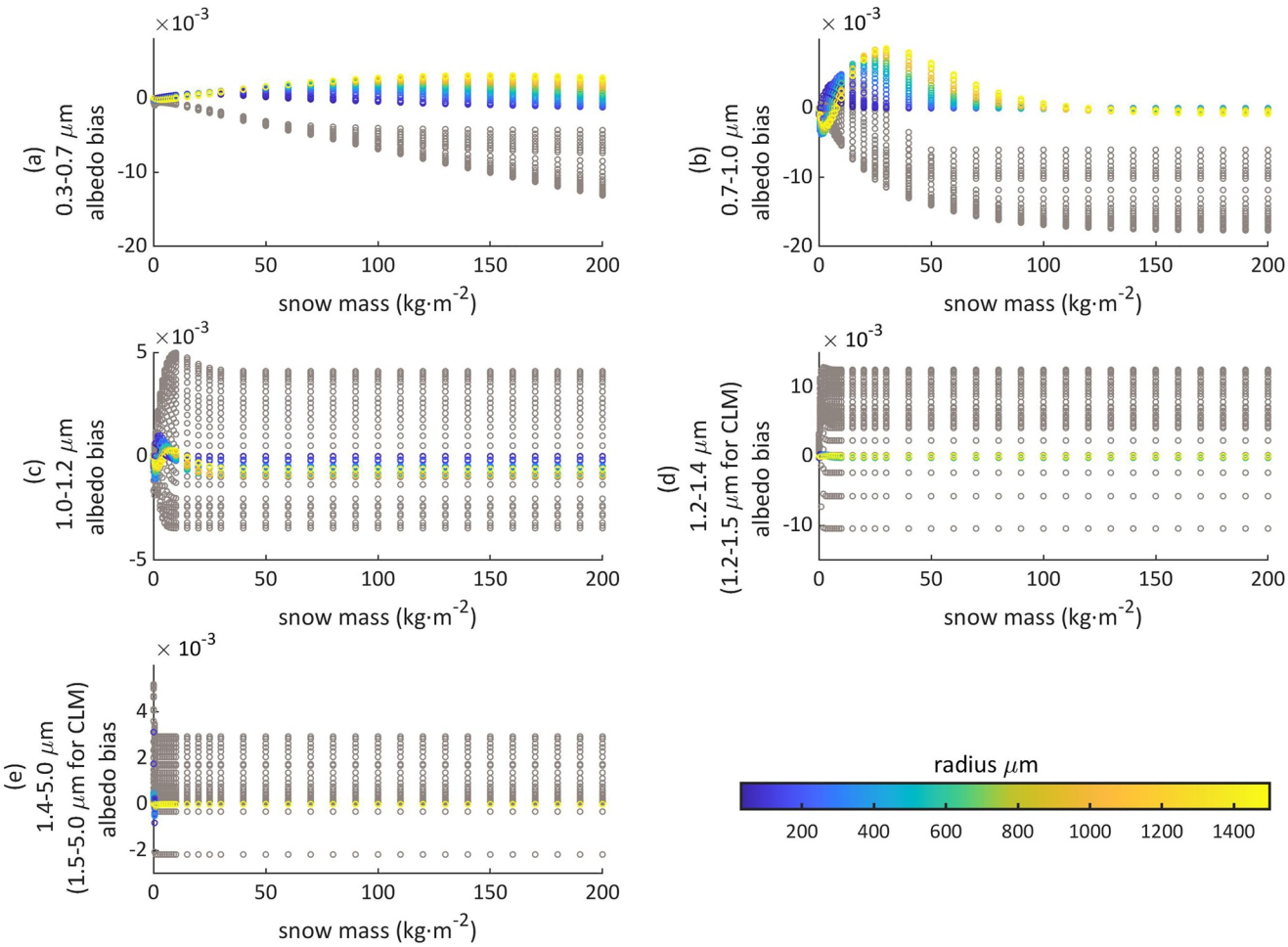

Figure 8. Same as Figure 7, but for cloudy sky albedo.

the new parameters is 0.002, equivalent to 0.6 Wm^{-2} in terms of the incoming solar energy, compared with the albedo bias of 0.004 in CLM, equivalent to 1.2 Wm^{-2}.

The constrained bias in the narrowband snow optical parameters improves the ability of LSMs to describe the impact of LAPs on snow ablation. Although the bias of the default narrowband snow optical parameters is limited as shown in Figure 2 and Tables 1 and 2, however, the LAP-induced snow albedo change is around 0.01 in the Arctic and North America (Dang et al., 2017) and so the improvement in the narrowband parameters is worthwhile to account for LAP impacts in these regions.

For wavelength-dependent Mie optical properties, the scattering properties of different snow grain shapes only differ in the asymmetry factor (He & Flanner, 2020). We assume this also holds for the narrowband parameters as described in Section 4.2. The derived parameters of spheroidal, hexagonal plate and Koch snowflake grain shape for the 0.3–0.7, 0.7–1.0, 1.0–1.2, and 1.2–1.4 μm band are as effective as that of spherical grain shape under both the clear and cloudy sky. The snow albedo biases using the narrowband parameters of the 1.4–5.0 μm band under the clear sky are within 2×10^{-3}, but under a cloudy sky this can increase to 0.025 for snow grain radius <200 μm. The larger bias in the 1.4–5.0 μm band parameters under a cloudy sky is due to the nonlinearity and can be constrained by directly applying Equations 17–19, however, the flux weight for the band is only 0.036 (Table 2), and the impact of the bias on the solar band is <0.001.

The difference of the new parameters from the default ones used in CLM is small (Table 3), but could produce albedo difference as large as shown in Figures 7 and 8. The contrast between the small difference of snow optical parameters and significant albedo bias indicates that it is the nonlinear combination of single scattering albedo,

Table 3
First Three Narrowband Snow Optical Parameters for Spherical Snow Grain of 200 and 1,000 μm

		0.3–0.7 μm		0.7–1.0 μm		1.0–1.2 μm	
	Radius (μm)	CLM	NEW	CLM	NEW	CLM	NEW
ω	200	0.9999	0.9999	0.9994	0.9994	0.9953	0.9953
	1,000	0.9998	0.9999	0.9972	0.9975	0.9781	0.9775
g	200	0.8902	0.8896	0.8927	0.8926	0.8944	0.8930
	1,000	0.8913	0.8911	0.8947	0.8961	0.8991	0.8991
e m^2•kg^{-1}	200	8.2258	8.1878	8.2445	8.0952	8.2569	8.0943
	1,000	1.6390	1.6365	1.6401	1.6075	1.6410	1.6084

Note. Both the parameters used in CLM ("CLM") and promoted in this study ("NEW") are presented for comparison.

asymmetry factor, and extinction cross section determines the snow albedo, not any of them alone.

We examine the accuracy of the derived narrowband LAP optical parameters by comparing the albedo bias of snow containing LAPs with that of pure snow in Figure 9. The bias of the estimated dirty snow albedo using the new parameters is 10 times smaller than that using the parameters in CLM. More specifically, the mode of the simulated snow albedo bias using the new parameters is closer to 0 for BC-loaded snowpack (Figures 9b and 9c), than using parameters in CLM. The snow albedo bias ranges from -1×10^{-3} to 12×10^{-3} for dirty snow (Figure 9d) using the parameters in CLM, while the dirty snow albedo bias is within $\pm 4 \times 10^{-3}$ when using the new parameters derived in this study.

5.2. Uncertainty From Spectrum of Incident Solar Flux

The narrowband snow optical parameters change with variations in the incident solar spectra under different atmospheric aerosol, cloud, and water vapor conditions. Theoretically, there should be different sets of narrowband snow optical parameters for the various spectra of incident flux, but this is not practical in climate models. Fortunately, the narrowband albedo bias caused by the variation of spectrum is very limited (<0.005) under both clear sky (Figure 10) and cloudy sky conditions (Figure 11).

Using the clear sky spectrum of midlatitude winter (MLW) with a solar zenith angle of 60° (MLW-60) as the default clear sky spectrum, the narrowband albedo bias from the albedo using other clear sky spectra with solar zenith angle varying from 10° to 80° is less than 0.005 (Figure 10), considering spectra representing the atmospheric conditions in midlatitude summer (MLS), tropical (TRP), high mountain (HMN), subarctic winter (SAW), subarctic summer (SAS), summit Greenland (SMM), and MLW. Similar biases in narrowband albedo are seen for the cloudy-sky condition of these typical spectra (Figure 11).

The uncertainty in the estimated clear sky broadband snow albedo integrated across the entire solar spectrum due to the changes in spectra with different water vapor conditions and solar zenith angles is 1×10^{-3} for thin snow with snow mass <10 kg•m^{-2} and 3.8×10^{-3} for thick snow. The uncertainty in the estimated cloudy sky broadband snow albedo due to the changes in atmospheric conditions is 1×10^{-3} for thin snow with mass <10 kg•m^{-2} and 2.5×10^{-3} for thick snow.

Directly applying the clear sky spectrum of MLW-60 as the cloudy sky spectrum will produce a diffuse albedo bias as large as 0.01 in the 0.7–0.9 μm band and 0.05 in the 1.4–5.0 μm band (not shown), with the corresponding solar broadband albedo bias as large as 0.005. Although this magnitude is relatively small, we would like to emphasize that both the narrowband snow optical parameters and hence narrowband albedo are spectrum-dependent.

5.3. Uncertainty From SNICAR

SNICAR itself has some uncertainties, for example, using two-stream approximations, without consideration of the ice lens effect from refreezing meltwater. Different two-stream approximations can produce variable snow albedo biases at different wavelengths, with changing solar zenith angle and snow depth (Dang et al., 2019). However, the evaluation in this study shows that the derived narrowband parameters are independent of the two-stream approximations (Section 5.1). Therefore, future improvement in two-stream approximations will broaden the application of the narrowband parameters derived in this study.

SNICAR does not consider liquid meltwater or the ice lensing effect of refreezing water. This, however, does not affect the parameter retrieval in this study. The effects of refreezing water and liquid meltwater can be included with further improvement in snow-aging parameterizations to represent the coupling between radiative transfer calculations and snow-aging processes (He & Flanner, 2020). We therefore conclude that the derived snow narrowband optical parameters are valid for most modeling circumstances.

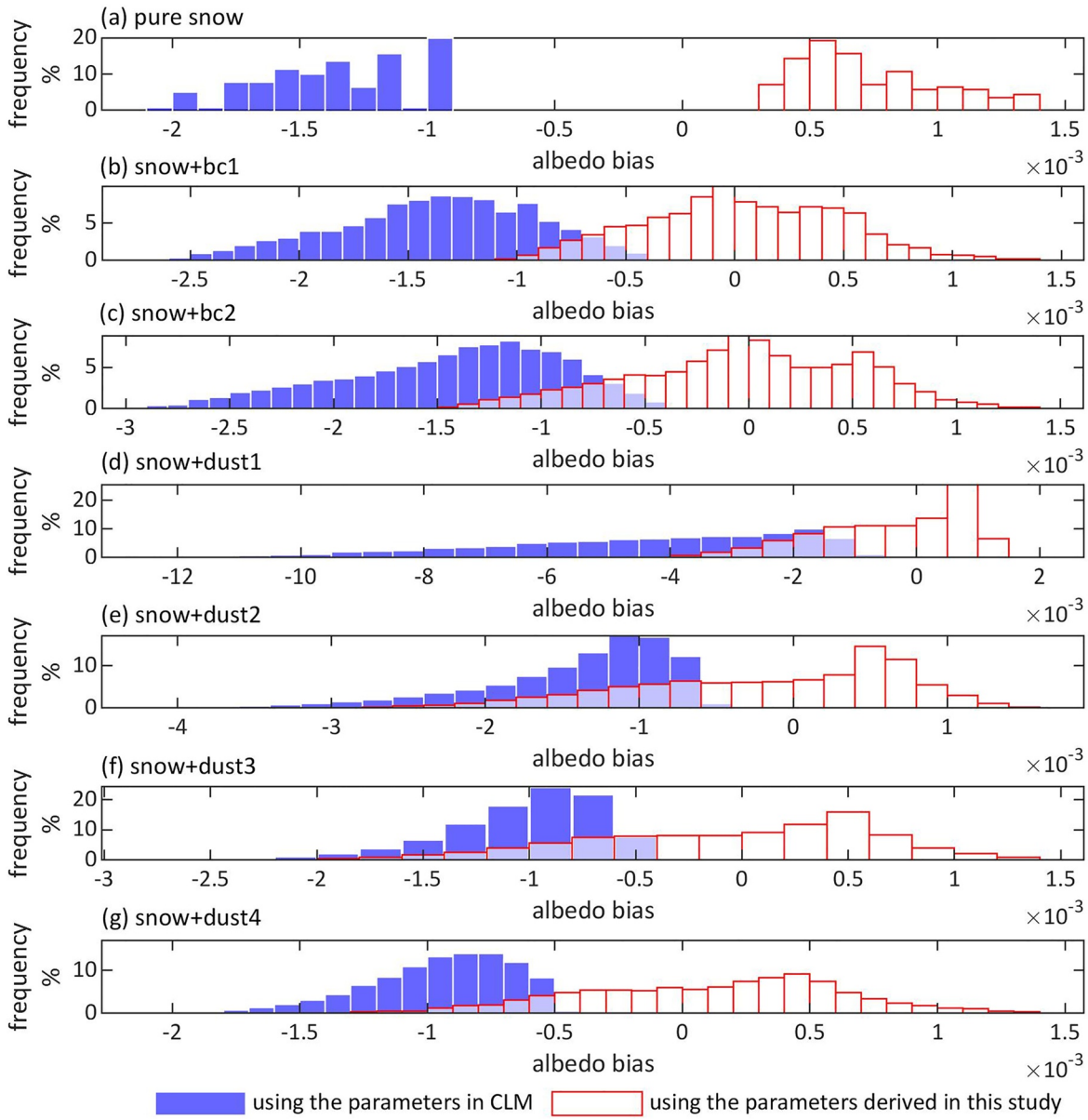

Figure 9. Bias distribution of snow albedo under clear sky at the 0.3–0.7 μm band for a 20 kg•m^{-2} snowpack at impurity concentrations within the typically observed ranges (e.g., Dang et al., 2017): black carbon (b–c) varies from 100 ng/g to 2,000 ng/g; mineral dust (d–g) varies from 5 μg/g to 100 μg/g. The cosine of the solar zenith angle varying from 0.15 to 0.95. The accuracy of the derived narrowband parameters are examined for all three two-stream approximations.

6. Summary and Implication

This study derived a new set of narrowband optical properties for both pure snow and snow containing LAPs, based on radiative transfer theory so as to maintain the accuracy of the spectrally resolved model (SNICAR). The derived narrowband optical parameters are robust and valid under various conditions with varying solar zenith angles, snow grain shapes, snow depths and densities, and LAP concentrations. The derived parameters are insensitive to different two stream approximations, and the sensitivity of the parameters to incident solar spectra is rather limited. The validation of the calculated narrowband snow albedo using the derived narrowband optical parameters against the spectrally resolved SNICAR simulations ensures high accuracy for both thin and thick snowpacks. These optical parameters are applicable to various land/climate models through updated look-up tables. Although the estimated narrowband snow albedo using the conventional irradiance-weighted narrowband

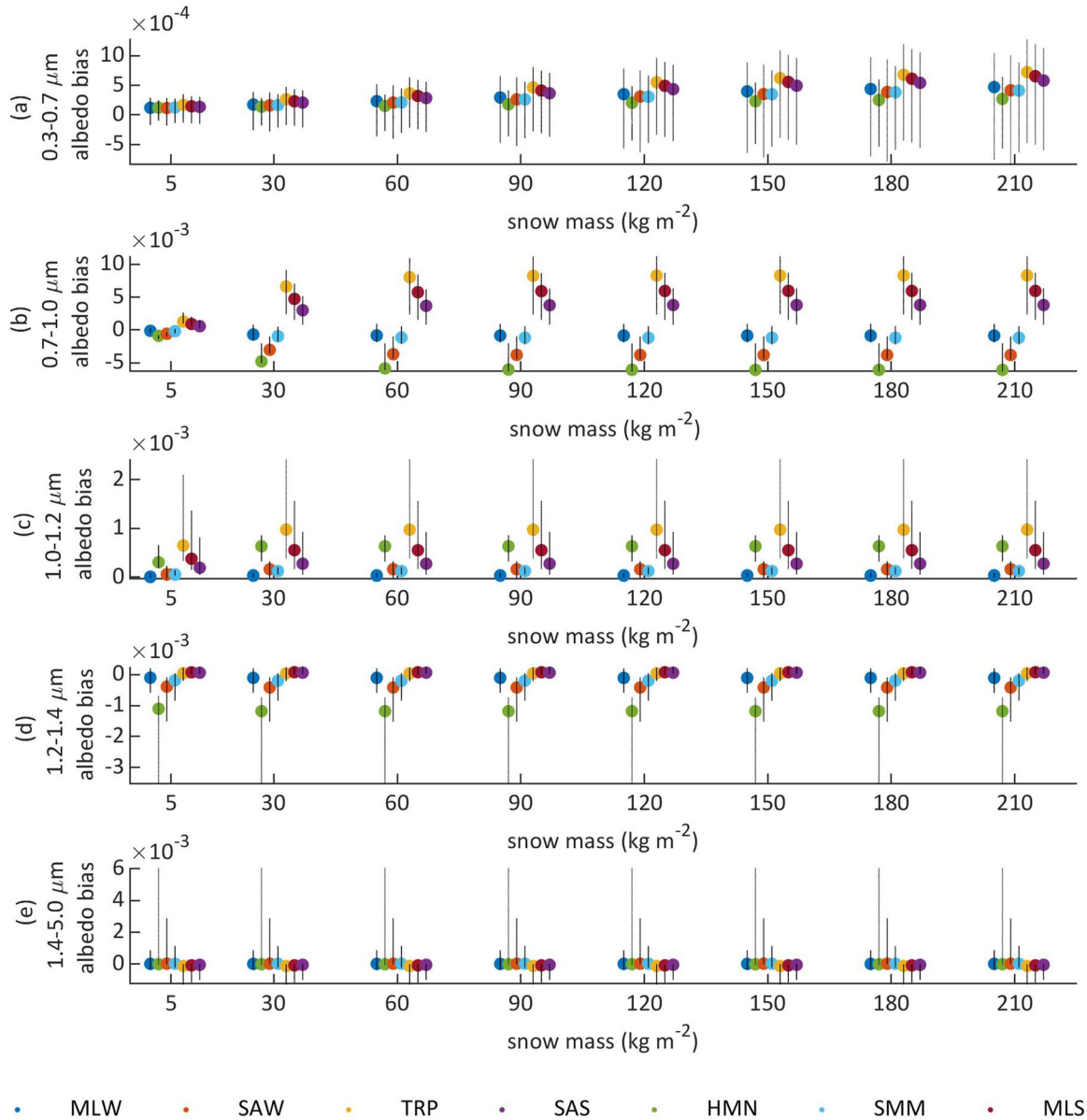

Figure 10. The bias of narrowband clear-sky snow albedo calculated using the midlatitude winter (MLW) spectrum with a solar zenith angle of 60° from using various other clear-sky incident solar spectra with solar zenith angle varying from 10° to 80°, including MLW, midlatitude summer (MLS), tropical (TRP), high mountain (HMN), subarctic winter (SAW), subarctic summer (SAS) and summit Greenland (SMM) spectral data obtained from the SNICAR database (https://github.com/mflanner/SNICARv3).

snow optical parameters in CLM are relatively accurate for thin snow (e.g., depth of 2 cm), the error rises up to 0.05 with the increase of snow mass/depth.

Climate change research should take into account the strong, positive snow-albedo feedback, processes affecting the snow state, for example, rising air temperatures, changing snow-to-rain ratio, and transport/deposition of LAPs by sand storms and emission of pollutants. To achieve this goal, physics-based snow albedo models to describe the radiative transfer incorporated with snow microphysics that affect snow optics are required. Preliminary efforts have been made to include more physically based snow albedo models (Flanner et al., 2007; Oleson et al., 2010). For example, the introduction of SNICAR into CLM makes it possible for global climate models to start consideration of the impact of black carbon or dust deposition on snow ablation (Flanner et al., 2007). However, the narrowband optical parameters of snow used in the snow radiative transfer schemes can be improved

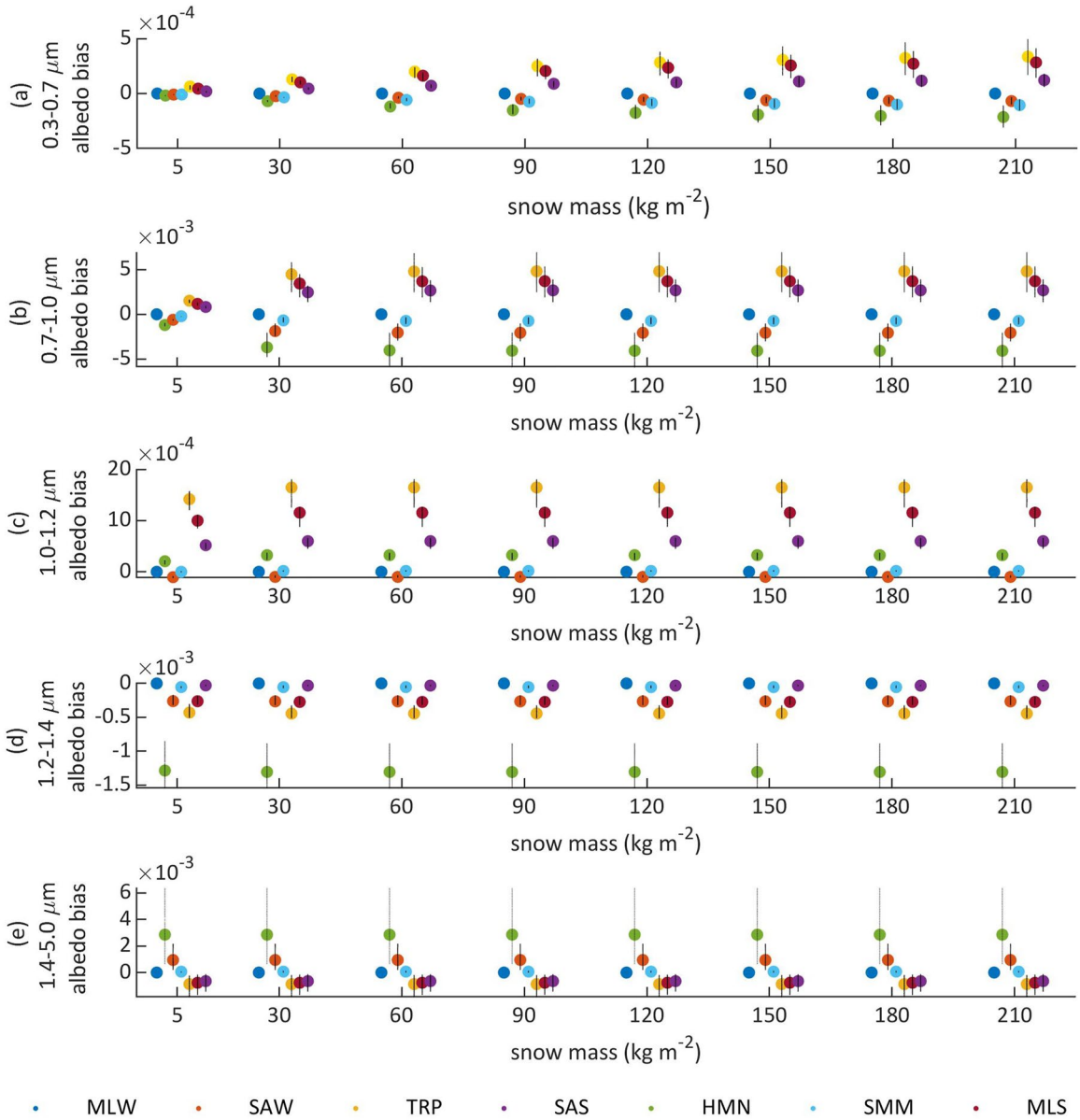

Figure 11. Same as Figure 10, but for cloudy-sky spectra.

and made more robust in various environments, by basing them more thoroughly on nonlinear radiative transfer theory.

Dang et al. (2017) evaluated the impact of black carbon and mineral dust on snow albedo, resulting in surface albedo changes of 0.008–0.02 in the Arctic and North American mountains, which are hotspots for studying the strong impact of various LAPs on snow under changing climates. To better resolve the impacts of LAPs, climate models need to improve the precision of albedo calculation to the level expected of LAP-induced albedo changes (0.008–0.02). The newly derived parameters in this study with an improved precision of albedo to the level of 10^{-3} are beneficial for climate models that resolve the impacts of LAPs.

We examined the effectiveness of the narrowband snow optical parameters given in Flanner et al. (2007) and currently used in CLM (Section 3). Their accuracy is acceptable for thin snowpacks but bias increases with snow thickness. How important are these biases in the land surface modeling could be resolved only with much work. It is true that uncertainties in various other processes may be greater in particular locations. However, the growth

of bias with the increasing snow mass implies inconsistent physics underlying the approximations used to derive the parameters currently in use. A better theoretical basis for the model parameters means more confidence in their application in a set of environmental conditions outside those where observations are plentiful. This applies not only to remote locations, but also to future scenarios where concentrations of LAP will vary from present day. Furthermore, climate change will produce large changes in snow season such as on the Arctic sea ice and Antarctic ice shelves. One method that is receiving increasing attention as a potential method of conserving the cryosphere involves the injection of light scattering aerosols into the stratosphere, with approximately 10 Tg/year of SO_2 (Kravitz et al., 2017; MacMartin et al., 2018) leading to a cooling of mean global temperature by 1°C. The Brewer-Dobson poleward circulation will lead to increased deposition of these particles onto snow packs thus potentially reversing the intended increases in snow season; high accuracy ESM and LSM snow models are the best tools able to address the net impact of these proposals.

The physics-based narrowband optical parameters of both snow grains and LAPs derived in this study are applicable in snow models and LSMs for both climate modeling and weather forecasting. Our derived optical parameters can be used to update the look-up tables in CLM used by the SNICAR radiative transfer scheme. The five-band snow albedo derived from the SNICAR calculations can further be integrated into the two-waveband LSMs, for example, Noah-MP (Niu et al., 2011) and CoLM (Dai et al., 2001) or single-waveband LSMs, for example, SSiB (Xue et al., 1991), with Equation 5.

The radiative transfer schemes that solve sunlight penetration at reduced narrow bands rather than at each of 470 wavelengths across the entire solar spectrum will improve the computation efficiency of climate models. The computational cost can be further reduced by applying analytical solutions to radiative transfer schemes rather than the tridiagonal matrix used in SNICAR. The general analytical solutions to the two-stream radiative transfer in snow has been developed (Wang, Moore, et al., 2021; attached in the uploaded files). The effective narrowband snow optical parameters derived in this study are used as lookup tables for the analytical solutions.

Data Availability Statement

The effective narrowband optical properties of pure snow and light-absorbing impurities produced in this work are available at https://doi.org/10.5281/zenodo.5555159.

Acknowledgments
This work was supported by the project of the National Key R&D Program of China (grant No. 2018YFA0606004), the National Science Foundation of China (Grant No. 41901075), and European Commission RIA No. 869471. The authors would like to emphasize our acknowledgment to Dr. Li Dan from Institute of Atmospheric Physics, Chinese Academy of Sciences, for his advice and special contribution to this manuscript.

References

Amaral, T., Wake, C. P., Dibb, J. E., Burakowski, E. A., & Stampone, M. (2017). A simple model of snow albedo decay using observations from the Community Collaborative Rain, Hail, and Snow-Albedo (CoCoRaHS-Albedo) Network. *Journal of Glaciology*, *63*(241), 877–887. https://doi.org/10.1017/jog.2017.54

Anderson, E. A. (1976). *A point energy and mass balance model of a snow cover*. *NOAA Technical Report NWS* (Vol.19, p. 150). Retrieved from http://amazon.nws.noaa.gov/articles/HRL_Pubs_PDF_May12_2009/HRL_PUBS_51-100/81_A_POINT_ENERGY_AND_MASS.pdf

Aoki, T., Hachikubo, A., & Hori, M. (2003). Effects of snow physical parameters on shortwave broadband albedos. *Journal of Geophysical Research*, *108*(D19), 4616. https://doi.org/10.1029/2003JD003506

Bohren, C. F., & Barkstrom, B. R. (1974). Theory of the optical properties of snow. *Journal of Geophysical Research*, *79*, 4527–4535. https://doi.org/10.1029/jc079i030p04527

Bohren, C. F., & Huffman, D. R. (1983). *Absorption and scattering of light by small particles*. Wiley.

Clarke, A. D., & Noone, K. J. (1985). Soot in the arctic snowpack: A cause for perturbations in radiative transfer. *Atmospheric Environment*, *19*, 2045–2053. https://doi.org/10.1016/0004-6981(85)90113-1

Dai, Y. J., Zeng, X., & Dickinson, R. E. (2001). *The Common Land Model (CLM): Technical documentation and user's guide* (p. 69). Georgia Institute of Technology.

Dang, C., Brandt, R. E., & Warren, S. G. (2015). Parameterizations for narrowband and narrowband albedo of pure snow and snow containing mineral dust and black carbon. *Journal of Geophysical Research*, *120*(11), 5446–5468. https://doi.org/10.1002/2014jd022646

Dang, C., Warren, S. G., Fu, Q., Doherty, S. J., Sturm, M., & Su, J. (2017). Measurements of light-absorbing particles in snow across the Arctic, North America, and China: Effects on surface albedo. *Journal of Geophysical Research: Atmospheres*, *122*, 10149–10168. https://doi.org/10.1002/2017JD027070

Dang, C., Zender, C. S., & Flanner, M. G. (2019). Intercomparison and improvement of two-stream shortwave radiative transfer schemes in Earth system models for a unified treatment of cryospheric surfaces. *The Cryosphere*, *13*, 2325–2343. https://doi.org/10.5194/tc-13-2325-2019

Déry, S. J., & Brown, R. D. (2007). Recent Northern Hemisphere snow cover extent trends and implications for the snow-albedo feedback. *Geophysical Research Letters*, *34*(22). https://doi.org/10.1029/2007GL031474

Doherty, S. J., Dang, C., Hegg, D. A., Zhang, R., & Warren, S. G. (2014). Black carbon and other light-absorbing particles in snow of central North America. *Journal of Geophysical Research: Atmospheres*, *119*, 12807–12831. https://doi.org/10.1002/2014JD022350

Doherty, S. J., Grenfell, T. C., Forsström, S., Hegg, D. L., Brandt, R. E., & Warren, S. G. (2013). Observed vertical redistribution of black carbon and other insoluble light-absorbing particles in melting snow. *Journal of Geophysical Research: Atmospheres*, *118*, 5553–5569. https://doi.org/10.1002/jgrd.50235

Flanner, M. G., & Zender, C. S. (2005). Snowpack radiative heating: Influence on Tibetan Plateau climate. *Geophysical Research Letters*, *32*, L06501. https://doi.org/10.1029/2004GL022076

Flanner, M. G., Zender, C. S., Hess, P. G., Mahowald, N. M., Painter, T. H., Ramanathan, V., & Rasch, P. J. (2009). Springtime warming and reduced snow cover from carbonaceous particles. *Atmospheric Chemistry and Physics*, *9*, 2481–2497. https://doi.org/10.5194/acp-9-2481-2009

Flanner, M. G., Zender, C. S., Randerson, J. T., & Rasch, P. J. (2007). Present day climate forcing and response from black carbon in snow. *Journal of Geophysical Research*, *112*, D11202. https://doi.org/10.1029/2006jd008003

Fletcher, C. G., Zhao, H., Kushner, P. J., & Fernandes, R. (2012). Using models and satellite observations to evaluate the strength of snow albedo feedback. *Journal of Geophysical Research*, *117*. https://doi.org/10.1029/2012JD017724

Fu, Q. (1996). An accurate parameterization of the solar radiative properties of cirrus clouds for climate models. *Journal of Climate*, *9*(9), 2058–2082. https://doi.org/10.1175/1520-0442(1996)009<2058:aapots>2.0.co;2

Gelman Constantin, J., Ruiz, L., Villarosa, G., Outes, V., Bajano, F. N., He, C., et al. (2020). Measurements and modeling of snow albedo at Alerce Glacier, Argentina: Effects of volcanic ash, snow grain size and cloudiness. *The Cryosphere*, *14*(12), 4581–4601. https://doi.org/10.5194/tc-14-4581-2020

Giddings, J. C., & LaChapelle, E. R. (1961). Diffusion theory applied to radiant energy distribution and albedo of snow. *Journal of Geophysical Research*, *66*, 181–189. https://doi.org/10.1029/jz066i001p00181

Hall, A., & Qu, X. (2006). Using the current seasonal cycle to constrain snow albedo feedback in future climate change. *Geophysical Research Letters*, *33*(3). https://doi.org/10.1029/2005GL025127

Hanesiak, J. M., Barber, D. G., & Flato, G. M. (1999). Role of diurnal processes in the seasonal evolution of sea ice and its snow cover. *Journal of Geophysical Research*, *104*, 13593–13603. https://doi.org/10.1029/1999JC900054

He, C., & Flanner, M. (2020). Snow albedo and radiative transfer: Theory, modeling, and parameterization. In A. Kokhanovsky (Ed.), *Springer Series in Light Scattering* (Vol. 5, pp. 67–133). Springer. https://doi.org/10.1007/978-3-030-38696-2_3

He, C., Flanner, M. G., Chen, F., Bariage, M., Liou, K. N., Kang, S., et al. (2018). Black carbon-induced snow albedo reduction over the Tibetan Plateau: Uncertainties from snow grain shape and aerosol–snow mixing state based on an updated SNICARmodel. *Atmospheric Chemistry and Physics*, *18*, 11507–11527. https://doi.org/10.5194/ACP-18-11507-2018

He, C., Liou, K. N., Takano, Y., Yang, P., Qi, L., & Chen, F. (2018). Impact of grain shape and multiple black carbon internal mixing on snow albedo: Parameterization and radiative effect analysis. *Journal of Geophysical Research: Atmospheres*, *123*, 1253–1268. https://doi.org/10.1002/2017JD027752

He, C., Takano, Y., Liou, K. N., Yang, P., Li, Q., & Chen, F. (2017). Impact of snow grain shape and black carbon-snow internal mixing on snow optical properties: Parameterizations for climate models. *Journal of Climate*, *30*(24), 10019–10036. https://doi.org/10.1175/JCLI-D-17-0300.1

Huang, J., Fu, Q., Zhang, W., Wang, X., Zhang, R., Ye, H., & Warren, S. G. (2011). Dust and black carbon in seasonal snow across northern China. *Bulletin of the American Meteorological Society*, *92*(2), 175–181. https://doi.org/10.1175/2010bams3064.1

Jin, Z., Charlock, T. P., Yang, P., Xie, Y., & Miller, W. (2008). Snow optical properties for different particle shapes with application to snow grain size retrieval and MODIS/CERES radiance comparison over Antarctica. *Remote Sensing of Environment*, *112*(9), 3563–3581. https://doi.org/10.1016/j.rse.2008.04.011

Kravitz, B., MacMartin, D. G., Mills, M. J., Richter, J. H., Tilmes, S., Lamarque, J. F., et al. (2017). First simulations of designing stratospheric sulfate aerosol geoengineering to meet multiple simultaneous climate objectives. *Journal of Geophysical Research*, *122*, 12616–12634. https://doi.org/10.1002/2017jd026874

Li, X., Kang, S., He, X., Qu, B., Tripathee, L., Jing, Z., et al. (2017). Light-absorbing impurities accelerate glacier melt in the central Tibetan Plateau. *Science of the Total Environment*, *587*, 482–490. https://doi.org/10.1016/J.SCITOTENV.2017.02.169

Liou, K. N., Takano, Y., He, C., Yang, P., Leung, L. R., Gu, Y., & Lee, W. L. (2014). Stochastic parameterization for light absorption by internally mixed BC/dust in snow grains for application to climate models. *Journal of Geophysical Research: Atmospheres*, *119*, 7616–7632. https://doi.org/10.1002/2014JD021665

MacMartin, D. G., Ricke Katharine, L., & Keith, D. W. (2018). Solar geoengineering as part of an overall strategy for meeting the 1.5°C Paris target. *Philosophical Transactions of the Royal Society A: Mathematical, Physical and Engineering Sciences*, *376*(2119), 20160454. https://doi.org/10.1098/rsta.2016.0454S

Mahowald, N. M., Muhs, D. R., Levis, S., Rasch, P. J., Yoshioka, M., Zender, C. S., & Luo, C. (2006). Change in atmospheric mineral aerosols in response to climate: Last glacial period, preindustrial, modern, and doubled carbon dioxide climates. *Journal of Geophysical Research*, *111*, D10202. https://doi.org/10.1029/2005JD006653

Meador, W. E., & Weaver, W. R. (1980). Two-stream approximations to radiative transfer in planetary atmospheres: A unified description of existing methods and a new improvement. *Journal of the Atmospheric Sciences*, *37*(3), 630–643. https://doi.org/10.1175/1520-0469(1980)037<0630:TSATRT>2.0.CO;2

Ming, J., Wang, Y., Du, Z., Zhang, T., Guo, W., Xiao, C., et al. (2015). Widespread albedo decreasing and induced melting of Himalayan snow and ice in the early 21st century. *PLoS One*, *10*(6). https://doi.org/10.1371/JOURNAL.PONE.0126235

Niu, G. Y., Yang, Z. L., Mitchell, K. E., Chen, F., Ek, M. B., Barlage, M., et al. (2011). The community Noah land surface model with multi parameterization options (Noah-MP): 1. Model description and evaluation with local-scale measurements. *Journal of Geophysical Research*, *116*, D12109. https://doi.org/10.1029/2010JD015139

Oleson, K. W., Lawrence, D. M., Bonan, G. B., Flanner, M. G., Kluzek, E., Lawrence, P. J., et al. (2010). Technical description of version 4.0 of the Community Land Model. *NCAR Technical Note* (NCAR/TN-478+STR, p. 257). University Corporation for Atmospheric Research.

Painter, T. H., Barrett, A. P., Landry, C. C., Neff, J. C., Cassidy, M. P., Lawrence, C. R., et al. (2007). Impact of disturbed desert soils on duration of mountain snow cover. *Geophysical Research Letters*, *34*, L12502. https://doi.org/10.1029/2007GL030284

Räisänen, P., Kokhanovsky, A., Guyot, G., Jourdan, O., & Nousiainen, T. (2015). Parameterization of single-scattering properties of snow. *Cryosphere*, *9*(3), 1277–1301.

Rasmus, S. (2005). *Snow pack structure characteristics in Finland: Measurements and modelling* (Ph.D. dissertation, p. 237). University of Helsinki.

Scanza, R. A., Mahowald, N., Ghan, S., Zender, C. S., Kok, J. F., Liu, X., et al. (2015). Modeling dust as component minerals in the Community Atmosphere Model: Development of framework and impact on radiative forcing. *Atmospheric Chemistry and Physics*, *15*, 537–561. https://doi.org/10.5194/acp-15-537-2015

Toon, O. B., McKay, C. P., Ackerman, T. P., & Santhanam, K. (1989). Rapid calculation of radiative heating rates and photodissociation rates in inhomogeneous multiple scattering atmospheres. *Journal of Geophysical Research*, *94*, 16287–16301. https://doi.org/10.1029/JD094iD13p16287

Wang, W., Moore, J., Dan, L., Zheng, H., Yang, Z. L., Yong, L., et al. (2021). *Coupling the ESM-SNICAR snow radiative transfer scheme with land surface models*. JAMES. under review (B).

Wang, W., Yang, K., Zhao, L., Zheng, Z., Lu, H., Mamtimin, A., et al. (2020). Characterizing surface albedo of shallow fresh snow and its importance for snow ablation on the interior of the Tibetan Plateau. *Journal of Hydrometeorology*, *21*(4), 815–827. https://doi.org/10.1175/jhm-d-19-0193.1

Wang, W., Yang, Z.-L., Yang, K., Moore, J. C., Che, T., & Niu, G. Y. (2021). *Improved snow process simulation by a land surface model with a radiative transfer scheme*. JAMES. under review (A).

Wang, X., Doherty, S. J., & Huang, J. (2013). Black carbon and other light-absorbing impurities in snow across northern China. *Journal of Geophysical Research: Atmospheres*, *118*, 1471–1492. https://doi.org/10.1029/2012JD018291

Warren, S. G., & Clarke, A. D. (1990). Soot in the atmosphere and snow surface of Antarctica. *Journal of Geophysical Research: Atmospheres*, *95*, 1811–1816. https://doi.org/10.1029/jd095id02p01811

Wiscombe, W. J., & Warren, S. G. (1980). A model for the spectral albedo of snow. I: Pure snow. *Journal of the Atmospheric Sciences*, *37*(12), 2712–2733. https://doi.org/10.1175/1520-0469(1980)037<2712:amftsa>2.0.co;2

Xue, Y., Sellers, P. J., Kinter, J. L., III, & Shukla, J. (1991). A simplified biosphere model for global climate studies. *Journal of Climate*, *4*, 345–364. https://doi.org/10.1175/1520-0442(1991)004<0345:asbmfg>2.0.co;2

Zender, C. S. (1999). Global climatology of abundance and solar absorption of oxygen collision complexes. *Journal of Geophysical Research*, *104*, 24471–24484. https://doi.org/10.1029/1999JD900797

Zender, C. S., Bian, H., & Newman, D. (2003). Mineral Dust Entrainment and Deposition (DEAD) model: Description and 1990s dust climatology. *Journal of Geophysical Research*, *108*. https://doi.org/10.1029/2002JD002775

Zender, C. S., Bush, B., Pope, S. K., Bucholtz, A., Collins, W. D., Kiehl, J. T., et al. (1997). Atmospheric absorption during the Atmospheric Radiation Measurement (ARM) Enhanced Shortwave Experiment (ARESE). *Journal of Geophysical Research*, *102*, 29901–29915. https://doi.org/10.1029/97jd01781

Zhang, R., Hegg, D. A., Huang, J., & Fu, Q. (2013). Source attribution of insoluble light-absorbing particles in seasonal snow across northern China. *Atmospheric Chemistry and Physics*, *13*, 6091–6099. https://doi.org/10.5194/acp-13-6091-2013

Zhong, X., Kang, S., Zhang, W., Yang, J., Li, X., Zhang, Y., et al. (2019). Light-absorbing impurities in snow cover across Northern Xinjiang, China. *Journal of Glaciology*, *65*, 1–18. https://doi.org/10.1017/jog.2019.69